ResearchGate

See discussions, stats, and author profiles for this publication at: https://www.researchgate.net/publication/263943271

Novel Synthesis of LaFeO3 Nanostructure Dendrites: A Systematic Investigation of Growth Mechanism, Properties, and Biosensing for Highly Selective Determination of Neurotransmitter...

ARTICLE *in* CRYSTAL GROWTH & DESIGN · NOVEMBER 2012

Impact Factor: 4.89 · DOI: 10.1021/cg3014305

CITATIONS
23

READS
78

6 AUTHORS, INCLUDING:

K. Girija
-
17 PUBLICATIONS **146** CITATIONS
SEE PROFILE

Devanesan Mangalaraj
Bharathiar University
303 PUBLICATIONS **3,462** CITATIONS
SEE PROFILE

Chinnuswamy Viswanathan
Bharathiar University
53 PUBLICATIONS **382** CITATIONS
SEE PROFILE

Ponpandian Nagamony
Bharathiar University
105 PUBLICATIONS **1,982** CITATIONS
SEE PROFILE

Available from: Ponpandian Nagamony
Retrieved on: 25 January 2016

CRYSTAL GROWTH & DESIGN

Article

pubs.acs.org/crystal

Novel Synthesis of $LaFeO_3$ Nanostructure Dendrites: A Systematic Investigation of Growth Mechanism, Properties, and Biosensing for Highly Selective Determination of Neurotransmitter Compounds

S. Thirumalairajan,[†] K. Girija,[†] V. Ganesh,[‡] D. Mangalaraj,[†] C. Viswanathan,[†] and N. Ponpandian*,[†]

[†]Department of Nanoscience and Technology, Bharathiar University, Coimbatore - 641 046, India

[‡]Electrodics and Electro Catalysis Division, Central Electrochemical Research Institute (CSIR-CECRI), Karaikudi - 630 006, India

ABSTRACT: Single-crystalline novel $LaFeO_3$ dendritic nanostructures are synthesized by a well-controlled, surfactant-assisted facile hydrothermal process. The morphology of the material is investigated by high-resolution transmission and scanning electron microscopy. The crystal nature and chemical composition of $LaFeO_3$ dendritic nanostructures are revealed from the X-ray diffraction, Raman spectroscopy, and X-ray photoelectron spectroscopy. Structural characterizations imply the preferential growth along the [121] direction by oriented attachment of $LaFeO_3$ nanoparticles in the diffusion limit, leading to the formation of $LaFeO_3$ dendrites. The microscopic studies confirm the formation of dendrites with a length of 3−4 μm, a branch diameter of 80 nm, and a length of 1−1.5 μm. The possible growth mechanism of the dendritic morphology is discussed from the aspect of diffusion and oriented attachment based on experimental results. Further, the electrochemical measurements performed on $LaFeO_3$ dendritic nanostructures deposited on the surface of a glassy carbon electrode exhibit a strong promoting effect. The oxidation current is proportional to concentration in the linear range of 8.2×10^{-8} to 1.6×10^{-7} M with a detection limit of 62 nM at S/N = 3. Meanwhile, the sensor effectively avoids the interference of ascorbic acid and uric acid, and it is successfully applied to determine the dopamine formulations with high selectivity and sensitivity.

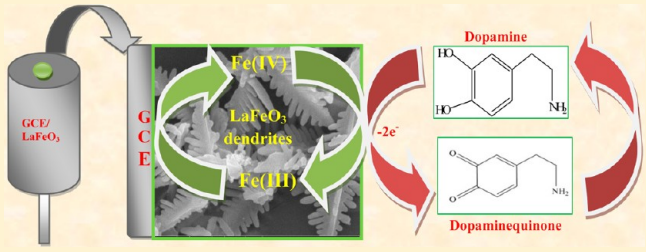

1. INTRODUCTION

Shape- and size-controlled synthesis of functional nanostructures, such as nanoparticles, nanocubes, nanospheres, nanowires, and nanorods, has gained importance as they exhibit unique electronic, optic, magnetic, and catalytic properties.[1−4] Especially, substantial attention has been focused on dendritic structures that can be applied in scientific and technological applications due to their large surface area and continuous networks.[5,6] In addition, the dendritic structures provide fundamental scientific opportunities for investigating the influence of size and dimensionality with respect to their collective novel properties and applications resulting from the spatial orientation and arrangement of nanoparticles. Generally, dendrite structures of metal oxide exhibit nonequilibrium growth processes that provide a natural framework for the study of disordered systems. Numerous theoretical and experimental results were reported, which contain information about the structure and growth mechanism of dendrites possessing promising complex functions, and their properties are highly dependent on the morphology.[7,8] The perovskite oxide with dendrite nanostructures also have many special characteristics, such as a large surface area composed of major trunks and branches. The preparation of dendritic structures with well-defined shapes may open new opportunities for wide applications in nanodevices.[9] Recently, a variety of dendrite crystals of metals,[10−12] metal oxides,[13] and chalcogenides[14] have been extensively studied theoretically and experimentally. Despite intensive experimental efforts, the dendritic structures of perovskite oxides have not been successfully obtained until now, which has hindered detailed experimental investigation of the morphology-dependent properties of these oxides. It is well-known that the properties of nanoparticles are dependent not only on their chemical composition but also on their structure, shape, and size. Therefore, the ability to tune the size and shape of $LaFeO_3$ nanostructures with tailored properties is significant for various investigations.

Over the past decade, many chemical methods, such as sol−gel, coprecipitation, combined polymerization, pyrolysis of metallo-organic precursors, and hydrothermal routes,[15−19] have been developed to prepare $LaFeO_3$ nanostructures with controlled physical and chemical characteristics. Among the various conventional techniques, the hydrothermal technique is an aqueous-based precipitation route allowing control over the nucleation, growth, and aging process. Surfactants as soft templates are involved in the formation of different morphologies by the self-assembly process. The combination of surfactant-assisted self-assembly under hydrothermal conditions has been used by many researchers to synthesize different morphologies.[20] The hexadecyltrimethyl ammonium bromide (CTAB) is used as a surfactant in the synthesis of

Received: September 28, 2012
Revised: November 15, 2012
Published: November 21, 2012

 © 2012 American Chemical Society dx.doi.org/10.1021/cg3014305 | *Cryst. Growth Des.* 2013, 13, 291−302

$LaFeO_3$ nanostructures, as it is an inexpensive organic stabilizer, needs no complicated procedure, is reactive at relatively low temperature, etc. The dendritic structures of $LaFeO_3$ samples were prepared and analyzed for their importance in interlinking fractals grown under nonequilibrium conditions and crystal growth phenomena. Until now, only few reports are available on the preparation and properties of perovskite dendritic nanostructures.[21,22]

The desire and important physiological analytes with high sensitivity has fueled the recent marriage between nanotechnology and biosensors. Nowadays, advances in biosensors based on nanostructured perovskite oxides are of practical importance in biological science, environmental science, neurochemistry, and biomedical chemistry.[23] L-Dopa, the precursor of dopamine (DA), is a chemical messenger produced within the nerve cell that is essential for the neurotransmission of the nerve impulse, and hence, the dysfunction in the central nervous dopamine system can lead to diseases, such as Parkinson's and schizophrenia. In vitro, dopamine is a powerful toxin to the culture of neurons and may also be toxic in vivo, according to some animal studies.[24] Therefore, the determination of DA has attracted much attention of researchers. Furthermore, some biomolecules, such as uric acid (UA) and ascorbic acid (AA), have a similar oxidation potential as that of dopamine, and it shows serious interference during the determination of dopamine.[25] To overcome these problems and also considering cost evaluation, much attention has been turned toward perovskite oxide based nanomaterial modified glassy carbon electrodes as alternatives. However, to the best of our knowledge, the cost-effective novel $LaFeO_3$ dendritic nanostructures for dopamine biosensing application has not been explored in the open literature.

In our present work, for the first time, we report the synthesis of novel $LaFeO_3$ dendritic nanostructures consisting of highly ordered trunks and branches via a facile hydrothermal process. The formation mechanism of $LaFeO_3$ dendrite nanostructures was analyzed, and the role of surfactant in controlling the particle morphology was elucidated. The modified $LaFeO_3$ dendrite nanostructure based biosensors have good sensitivity, selectivity, and stability and a low detection limit of dopamine, monitored through cyclic voltammetric and amperometric measurements.

2. EXPERIMENTAL SECTION

2.1. Material Preparation. Dendrite nanostructures of $LaFeO_3$ were synthesized by a simple hydrothermal process. All the chemicals, lanthanum nitrate hexahydrate $La(NO_3)_3{\cdot}6H_2O$, potassium ferric cyanide $K_3[Fe(CN)_6]$, and hexadecyltrimethyl ammonium bromide (CTAB) used were of analytical pure grade (99.99%). Stoichiometric amounts of $La(NO_3)_3{\cdot}6H_2O$ and $K_3[Fe(CN)_6]$ were dissolved in 30 mL of double-distilled water under magnetic stirring. An appropriate amount of CTAB was added to the solution. The concentration of surfactant CTAB was varied as 1:1:1, 1:1:2, and 1:1:3. In the typical experiment, the required quantity of CTAB was first dissolved in distilled water to form a solution of desired molar concentration and then added dropwise to the metal ion solution. The precursor solution was stirred magnetically for 30 min and then transferred to a Teflon-lined stainless steel autoclave for hydrothermal treatment maintained at 180 °C for 12 h. After the hydrothermal treatment, the autoclave was cooled naturally to room temperature. A light green colored precipitate settled at the bottom, which was collected and washed repeatedly with distilled water and ethanol to remove the impurities and excessive surfactant. The sample was finally dried at 100 °C for 12 h, followed by calcination at 800 °C for 2 h, to obtain $LaFeO_3$ powder for further characterization.

2.2. Characterization and Property Measurements. The surface morphology, chemical composition, particle size, and structure of the prepared nanostructures were characterized using scanning electron microscopy (SEM), energy-dispersive X-ray analysis (EDX) (SEM - JEOL JSM-6380LV), transmission electron microscopy (TEM, JEM 2100 F), performed with an acceleration voltage of 200 kV by placing the powder on a copper grid, and X-ray diffraction ((XRD), Bruker Germany D8 Advance) with Cu Kα radiation (λ = 1.54 Å). X-ray photoelectron spectroscopy (XPS) measurements were done on the ESCA + Omicron UK XPS system with a Mg Kα source and a photon energy of 1486.6 eV. All the binding energies were referenced to the C 1s peak at 284.6 eV of the surface adventitious carbon. The Raman spectrum was obtained for the prepared samples placed on a glass wafer using a LabRAM HR 800 Raman microscope with a 514 nm Ar-ion laser (10 mW). Fourier transformed infrared (FTIR) spectroscopy was performed on a Thermo Nicolet 200 FTIR spectrometer using the KBr wafer technique. A spectrum was collected in the mid-IR range from 400 to 4000 cm^{-1} with a resolution of 1 cm^{-1}. The thermal decomposition measurements of the prepared sample were determined from the simultaneous thermal analysis (TG/DTA, SDT Q 600 V20) from RT to 1000 °C under a nitrogen atmosphere. The Brunauer–Emmett–Teller (BET) isotherms of the powders were analyzed by nitrogen adsorption–desorption in a Micromeritics ASAP 2020. The prepared samples were degassed at 180 °C prior to nitrogen adsorption measurements. The isotherms were used to determine the pore size distribution by the Barrett–Joyner–Halenda (BJH) method.

2.3. Electrochemical Measurement. Electric signals were measured and recorded with a potentiostat-galvanostat electrochemical workstation (EG & G Instrument model 6310). The prepared solution was purged with nitrogen gas for 10 min prior to the electrochemical experiments. The electrochemical measurements were performed in a conventional two-compartment three-electrode cell with a mirror polished 0.07 cm^{-2} glassy carbon as the working electrode, Pt wire as the counter electrode, and 3 M KCl Ag/AgCl as the reference electrode. All the measurements were carried out in phosphate buffer solution (pH = 7.2) under a nitrogen atmosphere at room temperature.

3. RESULTS AND DISCUSSION

3.1. Impact of Calcination Temperature and CTAB Concentration on the Formation of $LaFeO_3$ Dendrites. The crystallinity and phase purity of the samples were determined using the powder XRD pattern for the as-prepared $LaFeO_3$ samples and those calcinated at different temperatures, as shown in Figure 1. The as-prepared sample shows an amorphous nature and is characterized by the broad continuum peaks.

The transformation of the amorphous phase to crystalline $LaFeO_3$ was not completed at 600 °C as it shows the presence of only a few characteristic peaks of $LaFeO_3$ with low intensity. When the calcination temperature was increased, the onset of $LaFeO_3$ crystallization can be observed, but with low intensity peaks at 700 °C. When the calcination temperature was increased to 800 °C, the high crystalline quality of perovskite-type $LaFeO_3$ samples was revealed. All the diffraction peaks can be indexed to the orthorhombic perovskite structure of $LaFeO_3$ with lattice constants a = 5.565 Å, b = 7.838 Å, and c = 5.577 Å within a maximum experimental error of ±0.0003, which is in accordance with the bulk $LaFeO_3$ crystals (JCPDS 37-1493). The strong and sharp diffraction peaks suggest that $LaFeO_3$ samples are highly crystalline and the spacing of the lattice fringes was 0.27 nm, well-indexed with the "d" spacing of the (121) plane of orthorhombic $LaFeO_3$ dendritic nanostructures from the HRTEM image discussed in the later section. No other peaks corresponding to La_2O_3/Fe_2O_3 or organic

dx.doi.org/10.1021/cg3014305 | Cryst. Growth Des. 2013, 13, 291–302

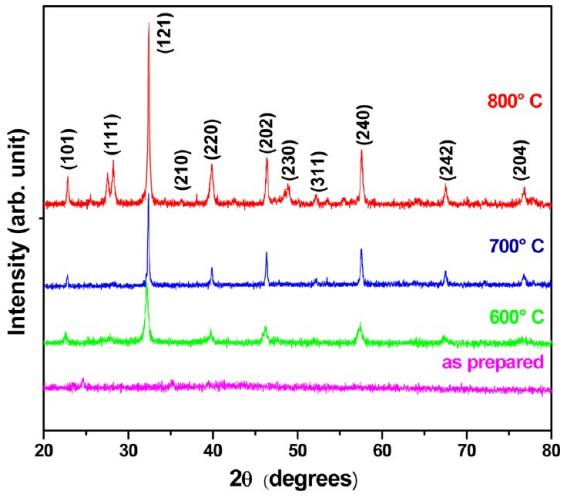

Figure 1. XRD pattern of nanostructured $LaFeO_3$ for different calcination temperatures.

impurities were present, which confirmed the presence of single-phase $LaFeO_3$. The diameter of crystallites calculated from the Williamson−Hall plot was used to calculate the average crystallite size using the Scherrer formula,[26] and it was found to be 84 nm. In addition, the percentage of crystallinity for 800 °C calcinated $LaFeO_3$ samples was estimated to be 82.4% from the XRD pattern.[27]

The surface morphology of the prepared $LaFeO_3$ samples was found to be different depending on the calcination temperature and CTAB concentration, as shown in Figure 2. Agglomerated nanoparticles were observed for the as-prepared $LaFeO_3$ samples, as shown in Figure 2a. The formation of $LaFeO_3$ nanoparticle based dendritic nanostructures with primary order branches started to grow at 600 °C calcination, as observed in Figure 2b. When the calcination temperature was increased, dendrites via the self-assembly process were observed at 700 °C, but crystallinity was not achieved, as shown in Figure 2c. When the calcination temperature was further increased to 800 °C (Figure 2d), a clear morphology with well-defined dendritic structures containing a main stem and branches was observed. The above results indicate that the

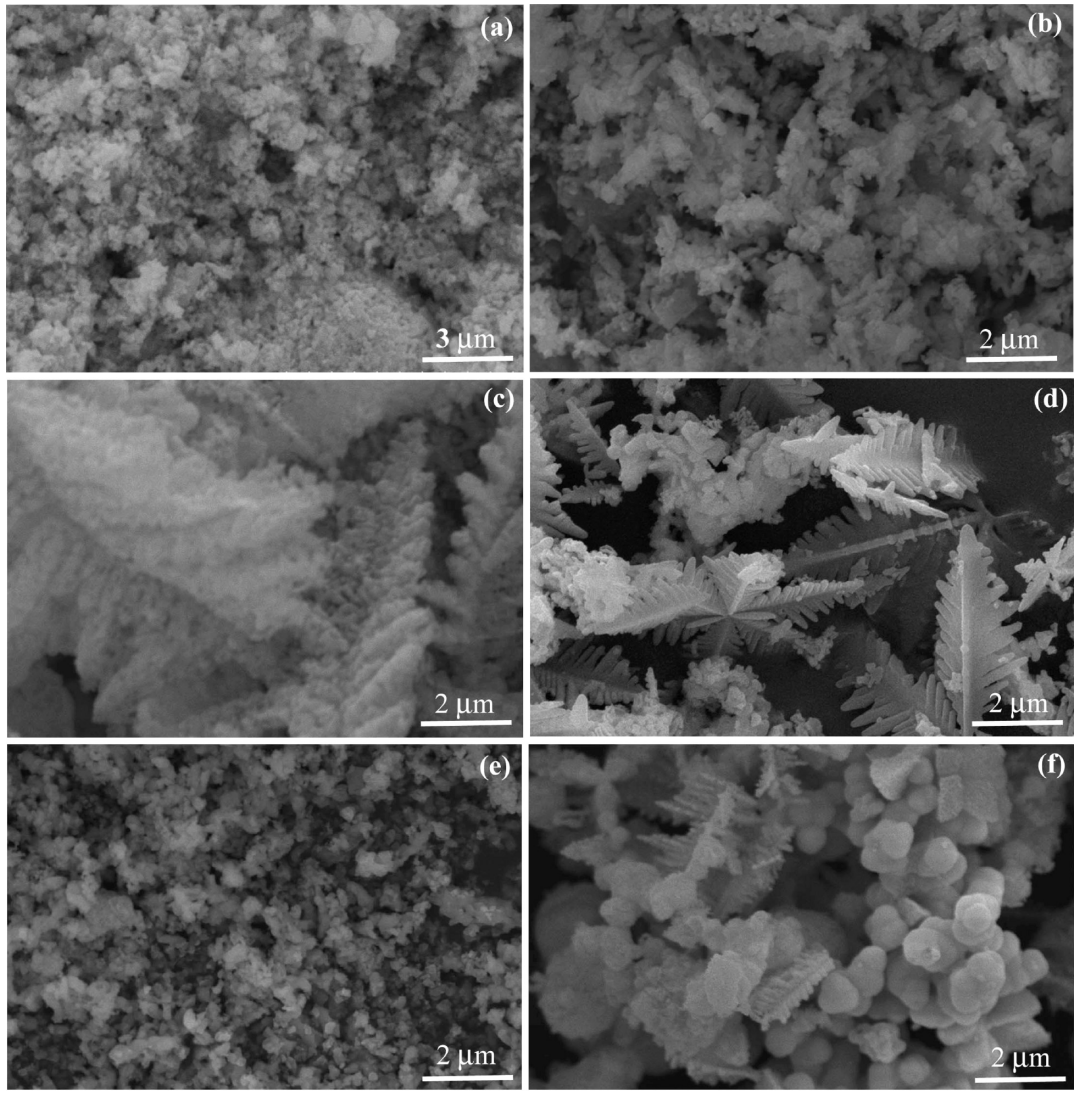

Figure 2. SEM images of (a) as-prepared, (b) 600 °C, (c) 700 °C, (d) 800 °C, and (e) low concentration and (f) high concentration of CTAB of $LaFeO_3$ dendritic nanostructures.

dx.doi.org/10.1021/cg3014305 | *Cryst. Growth Des.* 2013, 13, 291−302

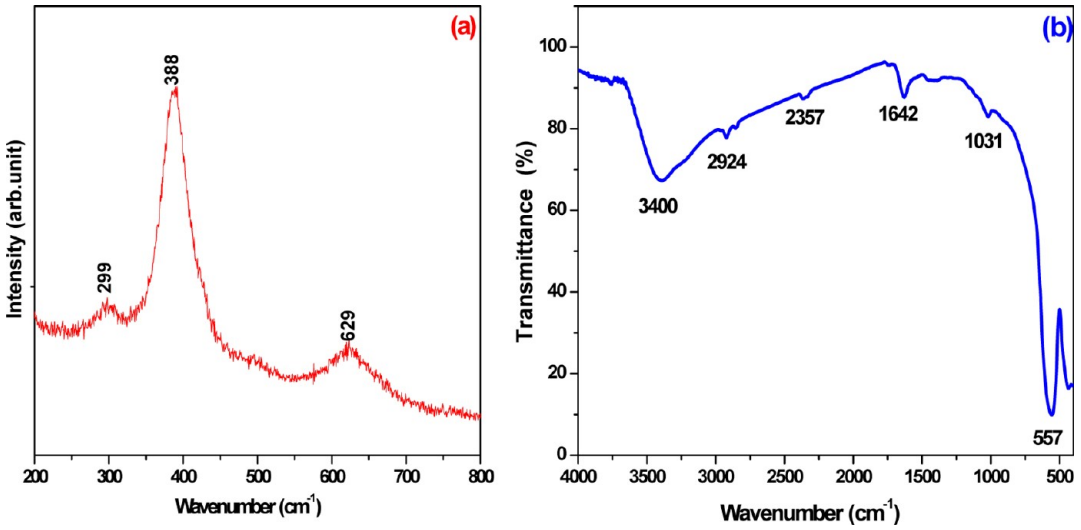

Figure 3. (a) Raman and (b) FTIR spectra of $LaFeO_3$ dendritic nanostructures.

calcination temperature is an important parameter in the formation of morphology and structure. To analyze the effect of CTAB surfactant on the final formation of nanostructure $LaFeO_3$ dendrites, we also have examined the influence of CTAB concentration on the morphology of $LaFeO_3$ in a hydrothermal process. The molar concentration of La/Fe/CTAB used were 1:1:1, 1:1:2, and 1:1:3, respectively. Aggregated nanoparticles were observed when a 1:1:1 molar concentration was employed in the typical synthesis process, as shown in Figure 2e. With a higher concentration of CTAB (1:1:3), more particles were arrested by the surfactant molecules, leaving behind very few particles for the dendritic formation. Thus, the use of excess surfactant hindered the formation of dendritic structures, resulting in spherical and incompletely formed branches, as shown in Figure 2f. A clear morphology and smooth surfaced $LaFeO_3$ dendrites observed in Figure 2d were formed when the La/Fe/CTAB molar concentration was 1:1:2 in the reaction solution, which indicates that an appropriate concentration of CTAB is a crucial prerequisite for the formation of perfect dendrites under selected hydrothermal reaction conditions.

The absorption of CTAB would direct the self-assembly of nanoparticles by molecular interaction into dendrites with certain crystallographic orientations. However, in the optimum precursor concentration, the diffusion is limited, and under this diffusion-limited regime, the growth proceeds further via oriented attachment of particles. The oriented attachment of particles starts with a seed particle formed by nucleation under supersaturation, and the growth of dendrites proceeds from this seed particle by the sticking and stacking of the diffusing particles at certain favorable sites determined by the crystal structure. This result is consistent with the observation that surfactant-assisted reaction is a simple and effective way to control the nucleation and growth process.[28] Finally, all the above results confirm that the calcination temperature finds importance for controlled growth of the dendrite structure. Hence, single-phase dendrite $LaFeO_3$ perovskite structures with a high crystalline quality, clear morphology formed at 800 °C with a CTAB concentration of 1:1:2 were used for further analysis and biosensing application in the present study.

The prepared $LaFeO_3$ dendritic nanostructures were further probed using Raman spectroscopy, which has the advantage of being very sensitive to structure distortion and oxygen motion. A detailed investigation of electron excitation is very important for determining the quality of crystalline samples and perovskite-type material structure. The room-temperature Raman spectrum of $LaFeO_3$ dendritic nanostructures is shown in Figure 3a. We observed three Raman modes for the orthorhombic $LaFeO_3$ structure at 299, 388, and 629 cm^{-1}. The two important modes at 299 and 629 cm^{-1} are due to A_g assigned modes, two-photon scattering, and impurity-related scattering. The B_{3g} assigned mode was observed at 388 cm^{-1}. The peak positions are in good agreement with the values reported for $LaFeO_3$.[29] No other peaks corresponding to lanthanum oxide and iron oxide were found, such as in the XRD pattern.

Further, the FT-IR spectrum was used to monitor the structure confirmation of $LaFeO_3$ dendrites shown in Figure 3b. The FTIR spectrum of the $LaFeO_3$ dendritic nanostructure was taken to complete the information of long-range order (XRD) with short-range order (Raman and FTIR). The broad band observed at 3400 cm^{-1} is characteristic of the H−O bending mode of absorbed water or the hydrogen bonded to the oxygen ions in the framework. In addition, the band observed at 2924 cm^{-1} corresponds to the physically absorbed CO_2, and the two bands at 2357 and 1642 cm^{-1} originate from the symmetric and asymmetric stretching of the carboxyl root. The smaller peak at 1031 cm^{-1} corresponds to the principal vibration of the CO_3^{2-} group due to the exposure to the ambient atmosphere, indicating that La-carbonate species exist on the $LaFeO_3$ surface of the perovskite compound, which was not detected in XRD. In addition, the intense band at 557 cm^{-1} can be attributed to the Fe−O stretching vibration being characteristic of the octahedral FeO_6 group in $LaFeO_3$. Contrarily, no obvious characteristic peaks of surface adsorbed oxygen species were observed. The results infer that the prepared $LaFeO_3$ has a carboxyl group, which is necessary for the development of biosensors. It can be thus concluded that the FTIR spectra of $LaFeO_3$ dendrites have similar structural units and formation of identical chemical moieties, as reported in the literature.[30] This is also in agreement with the results obtained from XRD and Raman analysis.

3.2. Composition Analysis. The elemental composition, purity, and chemical status of $LaFeO_3$ dendrites were carried

dx.doi.org/10.1021/cg3014305 | *Cryst. Growth Des.* 2013, 13, 291−302

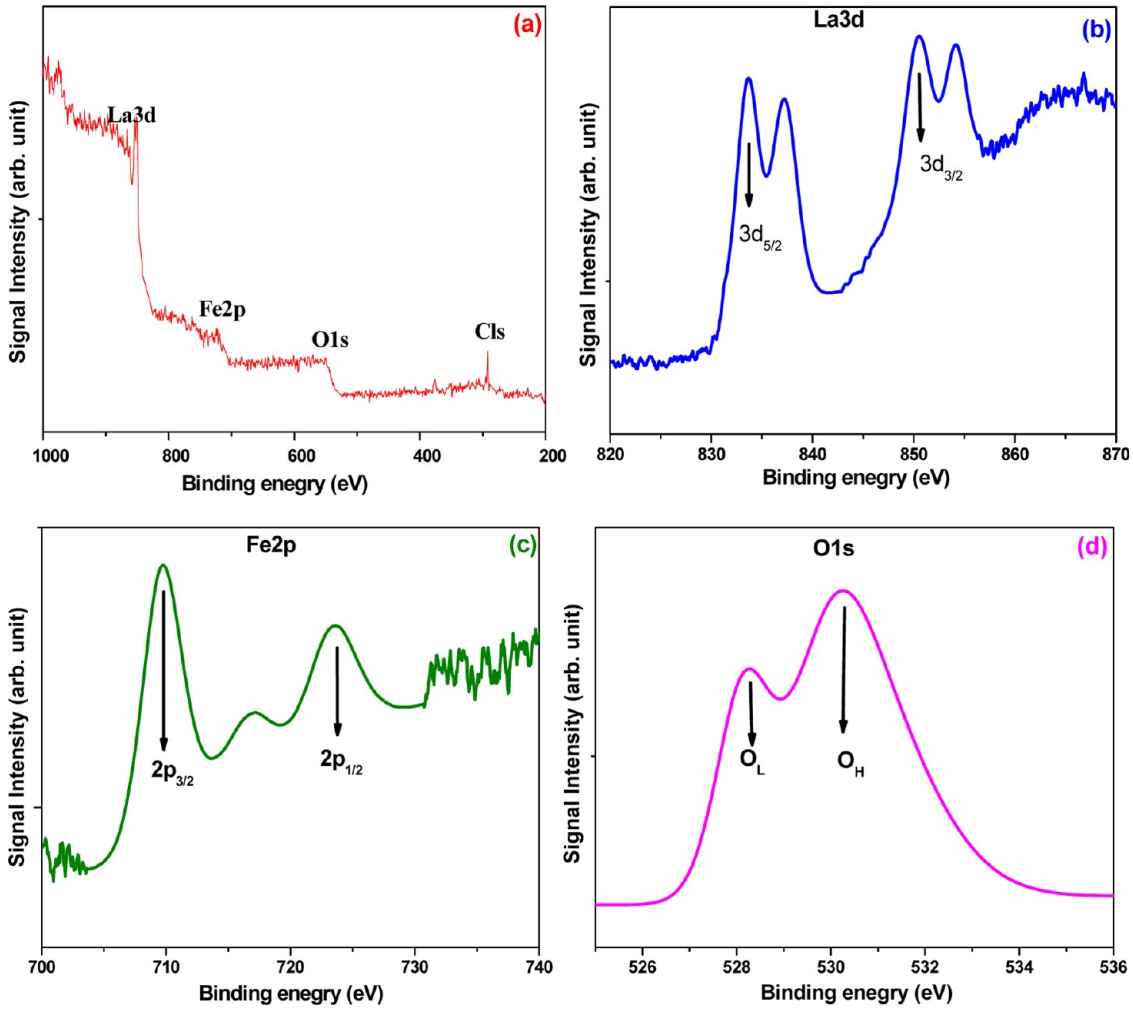

Figure 4. (a) XPS survey spectrum and (b) La 3d, (c) Fe 2p, and (d) O 1s spectra of $LaFeO_3$ dendritic nanostructures.

out using X-ray photoelectron spectroscopy. The binding energies obtained from the XPS analysis were corrected with the C 1s reference line at 284.6 eV. The typical XPS survey spectrum obtained from the dendritic $LaFeO_3$ morphology is shown in Figure 4a, which reveals the presence of La(3d), Fe(2p), O(1s), and C(1s). The carbon peak can be attributed to adventitious carbon on the surface of the samples. The XPS La 3d and Fe 2p core-level spectra reveal that, in $LaFeO_3$ samples, lanthanum and iron atoms are in the formal chemical valence state +3.[31] The high-resolution spectrum in Figure 4b shows that two strong La peaks were observed at 833.6 and 850.5 eV, which correspond to spin−orbit splitting of $3d_{5/2}$ and $3d_{3/2}$ of La^{3+} ions in oxide form. The binding energies of Fe $2p_{3/2}$ and Fe $2p_{1/2}$ were observed at 709.7 and 723.6 eV (Figure 4c), which correspond to Fe^{3+} ions in oxide form.[32] The two O 1s XPS spectra (Figure 4d) are wide and asymmetric, and it demonstrates that there are at least two kinds of O chemical states according to the binding energy at 528.2 eV ascribed to lattice oxygen species (OL) and 530.5 eV assigned to chemisorbed hydroxyl oxygen species (O^-) or OH^- species because the O(1s) binding energy of O^- or OH^- ion is generally higher by 2.1−2.5 eV than that of lattice oxygen.[33] Thus, the O 1s XPS spectrum is fitted to two kinds of chemical states by the Gaussian rule. The binding energy at 528.2 eV of the OL XPS signal can be attributed to the contribution of La−O and Fe−O in the $LaFeO_3$ crystal lattice. The OH XPS signal at 530.5 eV can be related to the hydroxyl group resulting mainly from the chemisorbed water, since lanthanum oxide is easily hygroscopic when exposed to air. From the relative intensities of the XPS spectra, the compositional stoichiometry was calculated between La, Fe, and O, and it was found to be about 1:1:3. This kind of metal−support interaction has been taken as an important factor in the biosensing analysis mechanism.

3.3. Thermal Analysis. Most of the perovskite oxide nanostructured materials may get dehydrated to some degree without major alternations in their crystal structure. Therefore, to evaluate the thermal stability of as-synthesized $LaFeO_3$ dendritic nanostructures, the thermal analysis was performed. Thermogravimetric analysis of $LaFeO_3$ dendrites was conducted from room temperature (RT) to 1000 °C with a heating rate of 20 °C/min, as shown in Figure 5. In the TG curve, 2.5 wt % of initial weight loss recorded from RT to 295 °C can be attributed to the evaporation of physically absorbed water, which is also evidenced from the exothermic peak at 290 °C in the differential thermal analysis (DTA) curve. As the temperature further increases, a notable weight loss of about 4.2% is observed between 295 and 380 °C; at the same time, the DTA curve shows an endothermic peak at 370 °C, which can be assigned to the decomposition of nitrates and other organic impurities.[34] A minor weight loss of 2.1% observed in the temperature range of 380−700 °C can be assigned to the

dx.doi.org/10.1021/cg3014305 | Cryst. Growth Des. 2013, 13, 291−302

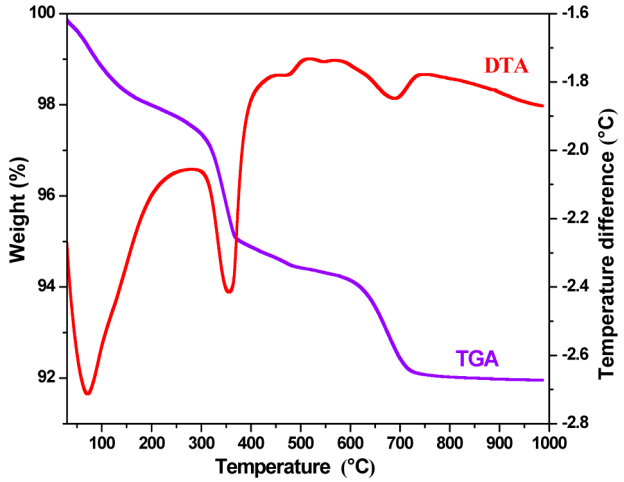

Figure 5. TG/DTA analysis of $LaFeO_3$ dendritic nanostructures.

complete decomposition of oxycarbonates. An endothermic peak observed at 670 °C can be possibly attributed to the decomposition of organics by oxidation and the release of NO_x, CO, and CO_2 gases, along with the gradual crystallization of $LaFeO_3$.[19] There was no weight loss detected by further increasing the temperature to 1000 °C. The TG/DTA curves gave strong evidence that the proposed molecular formula $LaFeO_3$ was rational. These observations are comparable to the results obtained from the XRD pattern of the as-prepared and calcinated samples (Figure 1), which confirms the transformation of amorphous to crystalline phase.

3.4. Morphological Analysis. The surface morphology of the prepared $LaFeO_3$ nanostructures was observed from the SEM image, as shown in Figure 6a, which clearly indicates the $LaFeO_3$ dendritic structures with a long main trunk and short side branches. Further observation of the high-magnification image in Figure 6b reveals the clear, well-defined, and uniformly ordered dendrite $LaFeO_3$ structures with a distinct trunk and branches distributed on both sides of the trunk. The overall length of the dendrite is about 3−4 μm, the average trunk diameter is 80 nm, and the branches are 1−1.5 μm in length with a diameter of 85 nm. The branches became shorter and shorter from the bottom to the tip of the stem, and no sub-branches were formed on the branches. The dendritic growth occurs at the tips of the stem and branches as the growth time increases. As the stem grows longer and longer, new branches were formed near the tip region continuously. For the higher-order branches (leaves), the dimension can reach as small as a few nanometers. Surprisingly and interestingly, all the side branches are flanked by the trunk symmetrically with an angle of ca. 60°, implying that the $LaFeO_3$ dendritic crystals grow along a preferential [121] direction. The $LaFeO_3$ nanoparticles with a size of around 80−90 nm, shown in Figure 6c, formed under supersaturation conditions, end up with dendritic structures due to an interplay between diffusion kinetics and

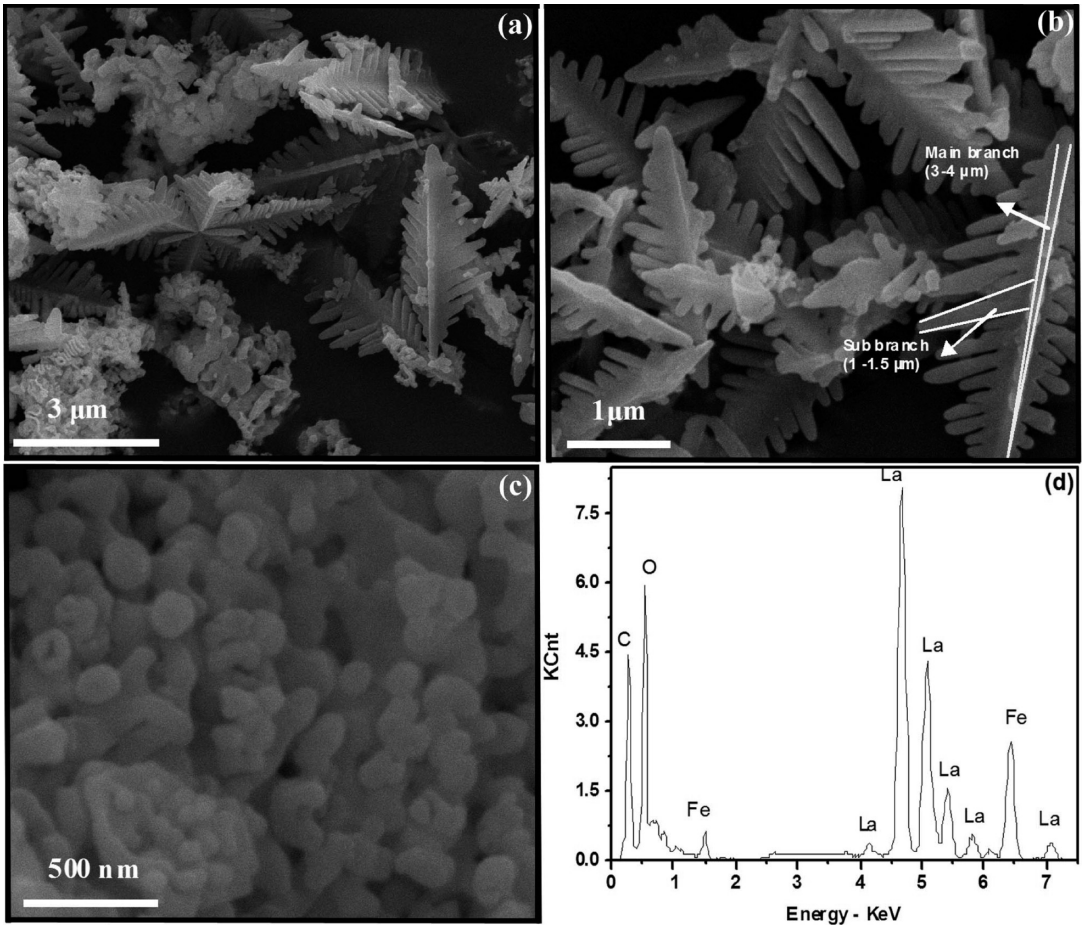

Figure 6. (a) Low-magnification and (b) high-magnification SEM images of $LaFeO_3$, view of dendrite main stem and branch, and (c) aggregation of $LaFeO_3$ nanoparticles. (d) EDAX pattern of $LaFeO_3$ dendritic nanostructures.

dx.doi.org/10.1021/cg3014305 | *Cryst. Growth Des.* 2013, 13, 291−302

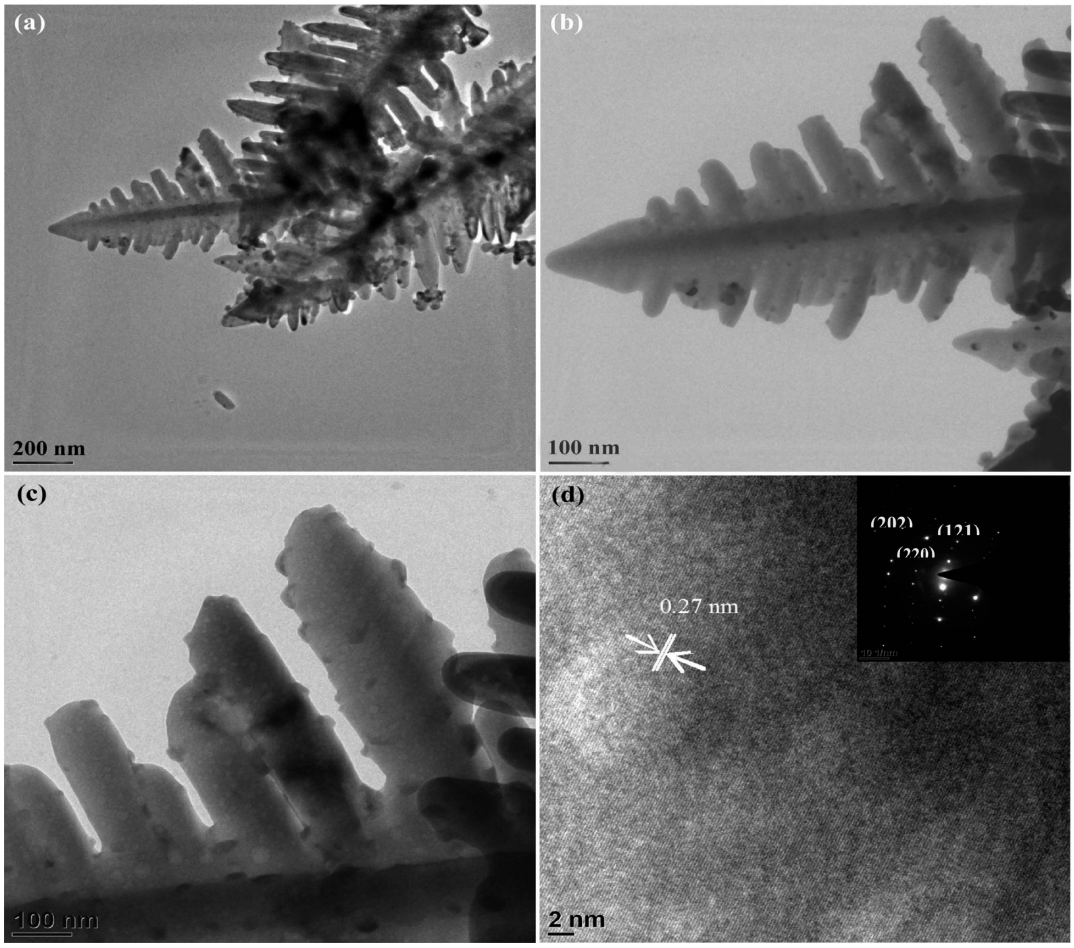

Figure 7. TEM images: (a) low-magnification, (b) high-magnification, and (c) branch. (d) HRTEM image of dendrites showing lattice fringes. (Inset) SAED pattern of $LaFeO_3$ dendritic nanostructures.

the oriented attachment of particles. The chemical composition of $LaFeO_3$ dendrites was also examined by energy-dispersive X-ray spectroscopy. As can be seen in Figure 6d, the elements present in the samples are La, Fe, and O with a molar ratio of 1:1:3 corresponding to the stoichiometric composition of $LaFeO_3$. The C peak in the spectrum can be attributed to the electric latex of the SEM sample holder. This is also in agreement with the result obtained from XPS analysis.

Further, the cationic surfactant CTAB ions absorbed on the surface of the $LaFeO_3$ particle directs the self-assembly process of nanoparticles by molecular interaction to form dendrites with certain crystallographic orientations. The surfactant not only provides favorable sites for the growth of particle assemblies but also influences the formation process, including nucleation, growth, coagulation, and flocculation. The surfactant was found to have a specific mechanism involved in the synthesis of nanostructures. During the synthesis process, the surfactants were absorbed by the growing crystal and, depending upon the precursor concentration and surfactant properties, they moderate the growth rate of crystal faces, which thereby helps in the shape and size control.[35] However, as the system is driven farther from equilibrium, dendritic growth can be promoted because the growth rate of crystals greatly exceeds the mass transport rate of ions that feed the growing crystals. In supersaturation-based crystallization, both the growth rate and the mass transport rate are governed by the concentration of the reactant.[36]

The TEM and HRTEM images in Figure 7 provide further insight into the prepared $LaFeO_3$ dendrites. The low-magnification TEM image (Figure 7a) reveals the high yield of $LaFeO_3$ dendrites and favorable uniformity achieved through this approach. A higher-magnification TEM image of a single dendrite is shown in Figure 7b, which clearly reveals the dendritic structure. The length of the $LaFeO_3$ dendritic trunk was ~3−4 μm. In Figure 7c, it is clear that the dendrite is highly symmetric, and the angle between stem and branches was about 60°. The length and diameter of the branches are 1−1.5 μm and ~85 nm, respectively. The HRTEM image recorded from the tip of the individual dendritic $LaFeO_3$ is shown in Figure 7d. The lattice fringes with the corresponding SAED pattern in the inset of Figure 7d indicate the single-crystalline nature due to the major diffraction spots corresponding to (121), (220), and (202). No diffraction spots were attributed to the secondary phase or impurity. Thus, by correlating the outcome from TEM and HRTEM images, it can be concluded that the observed results are in good agreement with SEM and XRD results.

3.5. Growth Mechanism and Influencing Factors. The growth mechanism of $LaFeO_3$ dendritic nanostructures can be determined by both the internal and the external conditions, such as calcination temperature and surfactant concentration. It is well-known that the shape of nanoparticles can be controlled by the surfactant, and the possible formation mechanism is as follows

dx.doi.org/10.1021/cg3014305 | *Cryst. Growth Des.* 2013, 13, 291−302

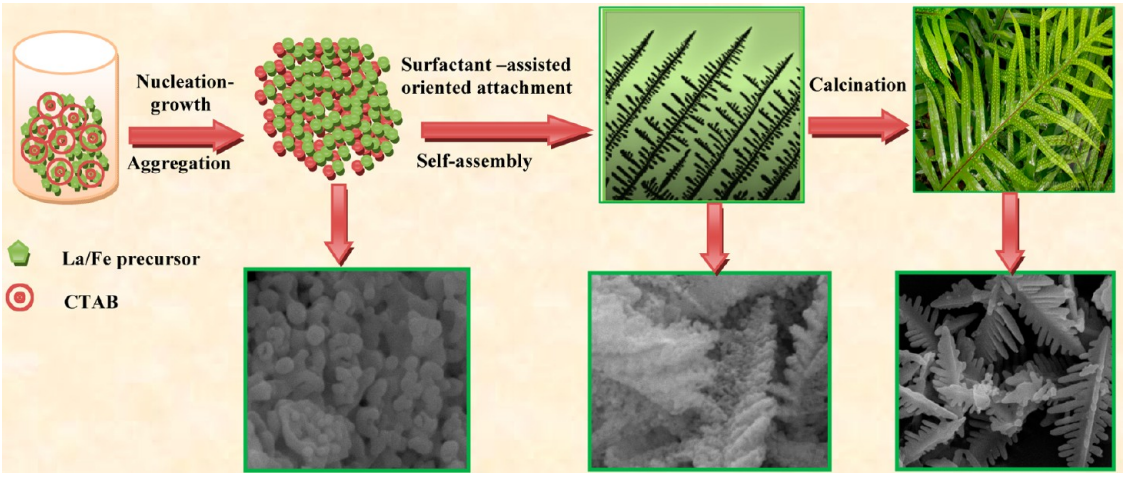

Figure 8. Schematic diagram illustrating the growth mechanism of $LaFeO_3$ dendritic nanostructures.

$$La(NO_3)_3 \rightarrow La^{3+} + 3NO_3^- \quad (1)$$

$$[Fe(CN_6)]^3 \rightarrow Fe^{3+} + 3OH^- \rightarrow Fe(OH)_3 \quad (2)$$

$$La^{3+} + C_{19}H_{42}BrN \rightarrow [C_6BrNH_{13}]^{3-}La^{3+} + 3H^+ \quad (3)$$

$$[C_6BrNH_{13}]^{3-}La^{3+} + 3OH^- \rightarrow La(OH)_3 + [C_6BrNH_{13}]^{3-} \quad (4)$$

$$La(OH)_3 + Fe(OH)_3 \rightarrow LaFeO_3 + 3H_2O \quad (5)$$

La^{3+} ions were produced when $La(NO_3)_3$ was dissolved in water (eq 1). $[Fe(CN_6)]^3$ dissociate into Fe^{3+} ions and further hydrolyze to form $Fe(OH)_3$ under hydrothermal reaction temperature as they are highly stable at room temperature (eq 2).[37] La^{3+} combines easily with CTAB via the chelating effect than Fe^{3+} owing to the much higher stability constant than the Fe^{3+} complex (eq 3). La^{3+} will be released slowly and gradually converted into $La(OH)_3$ via the alcoholysis reaction during the hydrothermal process (eq 4). The simultaneously formed $Fe(OH)_3$ react with $La(OH)_3$ to form the $LaFeO_3$ precipitates by the condensation effect (eq 5). The shape of the precursors plays a very important role on the final formation of dendritic $LaFeO_3$. It is known that CTAB not only accelerates the reaction speed of the growth units but also directs their oriented attachment: growth of diffusion-limited aggregation.

The formation process of $LaFeO_3$ dendritic nanostructures is speculated in Figure 8. The reaction temperature and precursor concentration significantly influence the morphology of the product, which has been discussed in the previous section. Nanostructured dendrites were obtained under hydrothermal optimized conditions, as in Figure 2d. These results suggest that the controlled size and shape of $LaFeO_3$ dendritic nanostructures can be obtained by controlling the kinetic parameters of the reaction process. At the initial stage, the slow dissociation nature of ions in the precursor solution and the controlled diffusion of $LaFeO_3$ arising due to the temperature and concentration gradient under hydrothermal conditions play an important role in the growth of dendritic structures. The precursor concentration (1:1:3) directly affects the growth of $LaFeO_3$ dendrites. The nanoparticles formed by nucleation under supersaturation conditions serve as an immobile seed in the solution. Some free nanoparticles from a random position far away diffuse toward the seed. Once they touch the seed, they are immobilized instantly on the empty surface of the seed, yielding an initial aggregate of $LaFeO_3$ nanoparticles (Figure 6c), with the seed as the center and the attached nanoparticle as the arm. With elapsed time, other free nanoparticles will diffuse continuously toward the aggregate and further be immobilized on the empty surface of the arm, forming a larger aggregate. This crystal growth process continues until all free nanoparticles are depleted, leading to the dendritic nanostructure. Actually, a large mass of seeds is distributed uniformly in the solution, and multiple aggregation events occur simultaneously in the respective regions of the solution. As a result, dendrites with limited sizes were obtained. The physical adsorption of diffusing $LaFeO_3$ crystals when contacted with each other leads to the formation of symmetrical dendrites. The growth of dendrites is globally diffusion-controlled, but locally accomplished by oriented attachment, which was found to be responsible for the formation of dislocations during early crystal growth.[38]

In equilibrium conditions, the crystal grown under these hydrothermal conditions may exhibit simple morphologies with minimum surface energy. In our case, as the system is driven farther from equilibrium, the growth rate of crystals exceeds the mass transport rate of ions that feed the growing crystal, leading to the formation of a main stem, and symmetric branches on both sides called dendrites were promoted. Therefore, it is reasonable to suggest that rapid nucleation and growth kinetics of $LaFeO_3$ nanoparticles contribute mainly to the formation of dendrites. The controlled growth of the dendrite system by a diffusive process can be related to the diffusion-limited aggregation (DLA) model developed to interpret this type of system.[39] The rate of nucleation and subsequent growths of dendritic nanostructures are effectively controlled by the hydrothermal reaction conditions and surfactant concentration.[40] This result is consistent with the observation that surfactant-assisted reaction is a simple and effective way to control the nucleation and growth process. The surfactant as a structure-directing agent has played a key role in the formation of $LaFeO_3$ dendritic nanostructures.

3.6. Specific Surface Area Analysis. The surface properties of biosensing materials are very important to achieving a good sensing performance. The surface area of $LaFeO_3$ nanostructures was measured from nitrogen adsorption−desorption isotherms using the BET and BJH methods. As can be seen in Figure 9a, $LaFeO_3$ dendrites exhibit a type-IV

dx.doi.org/10.1021/cg3014305 | *Cryst. Growth Des.* 2013, 13, 291−302

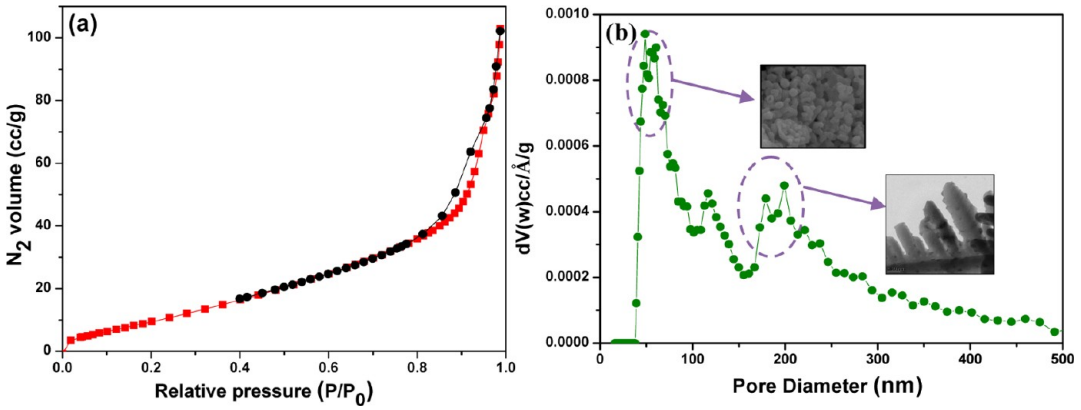

Figure 9. (a) Nitrogen adsorption–desorption isotherms and (b) the corresponding pore size distribution of $LaFeO_3$ dendritic nanostructures.

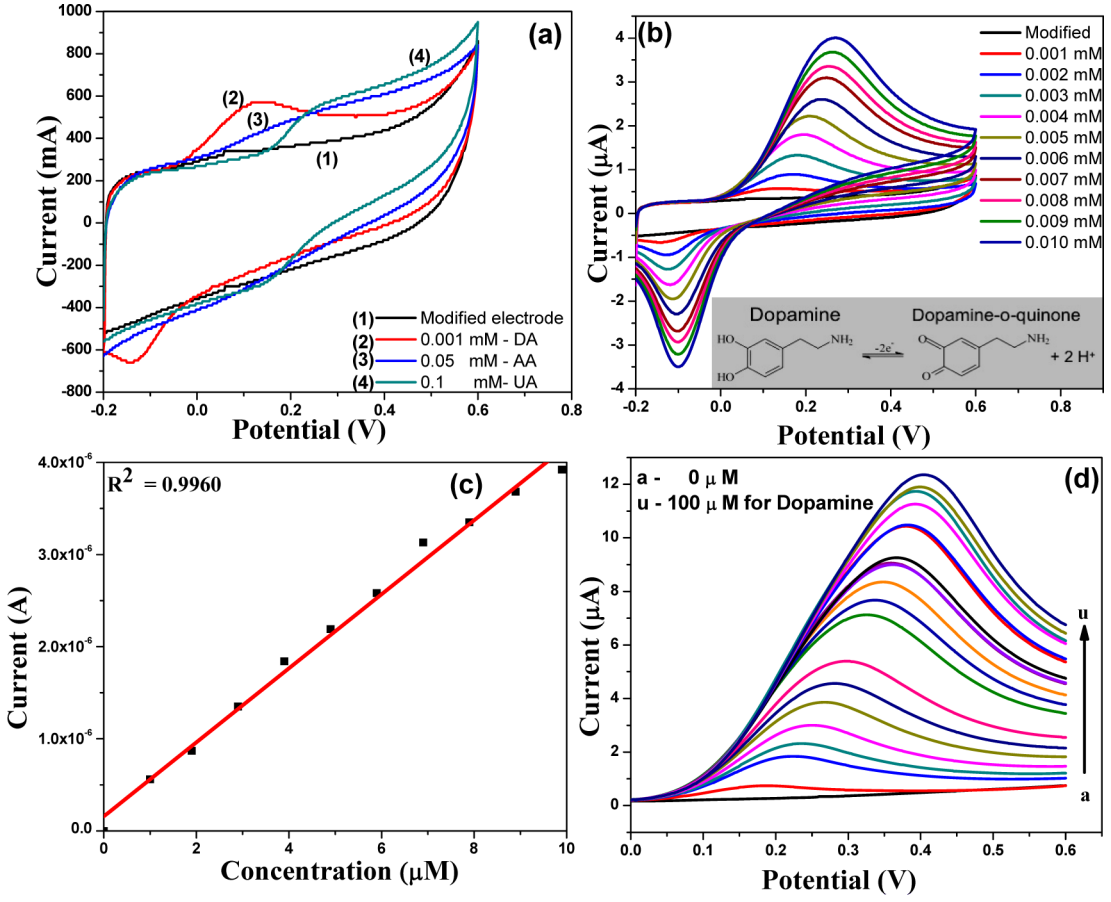

Figure 10. Cyclic voltammograms recorded for $LaFeO_3$ dendritic nanostructure modified electrode in PBS (10 mM, pH 7.2) at 50 mV s^{-1} for (a) low concentration of DA and high concentration of AA and UA and (b) different concentrations of DA (1–10 μM). (c) Plot of catalytic current vs the concentration of DA. (d) LSVs obtained for DA concentration range from 0 to 100 μM.

isotherm with a hysteresis loop in the high-pressure range ($0.8 < P/P_0 < 1$). The value of the BET specific surface area (SSA) was found to be 68.5 m^2 g^{-1}. It should be indicated that the dendrite structure itself does not exhibit a microporous structure. The pores can be ascribed to the interparticle space and the interbranch space. Moreover, the whole architecture is relatively large; the surface area can likely be contributed to the surface condition of the dendrites. The large surface area indicates that the $LaFeO_3$ dendritic nanostructures would possess a fascinating adsorbing ability to analytes in biosensing. It is really valuable to achieve an improved biosensing performance, such as high response and low detecting limit, which will be demonstrated in the later section. In addition, the Barrett–Joyner–Halenda (BJH) method was used to determine the pore volume of $LaFeO_3$ dendritic nanostructured samples (Figure 9b). In the pore size distribution curve, three different peaks can be clearly noticed. The first and second peaks positioned at 60 and 100 nm may correspond to the voids between the crystallites present in agglomerated particles. The presence of agglomerated particles in the $LaFeO_3$ material with varying sizes has been confirmed earlier in this study from the obtained SEM micrographs. The presence of crystallites

dx.doi.org/10.1021/cg3014305 | Cryst. Growth Des. 2013, 13, 291–302

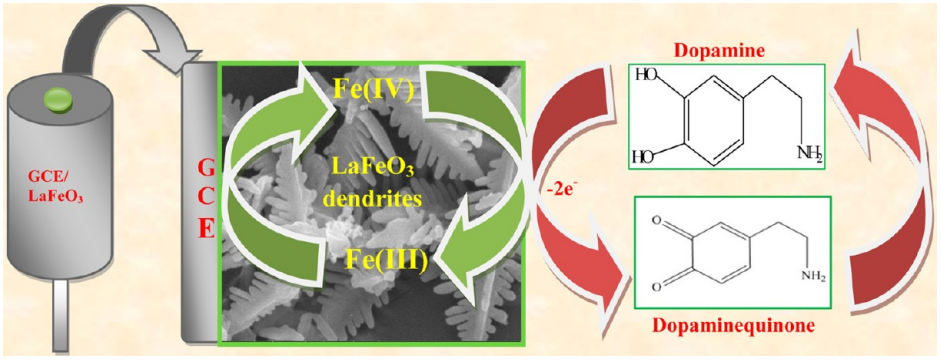

Figure 11. Schematic illustration of electrocatalytic dopamine oxidation at the $LaFeO_3$ dendrite nanostructure modified GCE.

within the aggregated particles was evidenced from the XRD results.

On the other hand, the third peak with a pore diameter of ~150 nm may correspond to the voids formed on the branches of dendrite nanostructures. The obtained results reveal that the as-synthesized $LaFeO_3$ dendrites have a microporous nature with a volume of 0.125 $cm^3\ g^{-1}$. This suggests that the prepared $LaFeO_3$ dendritic nanostructures could show high biosensing property because it is closely related to the morphology, surface area, and pore size distribution.

4. FABRICATION OF GLASSY CARBON ELECTRODE MODIFIED WITH $LAFEO_3$ DENDRITE NANOSTRUCTURES

The bare glassy carbon electrode was polished to a mirror-like surface with 0.05 μM alumina powder and sonicated in double distilled water for 10 min. A 100 mg portion of $LaFeO_3$ nanoparticles was dispersed in 10 mL of anhydrous alcohol and ultrasonicated for 30 min; 10 μL of alcoholic dispersed $LaFeO_3$ from the above solution was dropped onto the glassy carbon surface and air-dried at ambient temperature.

4.1. Electrocatalytic Properties of $LaFeO_3$ Dendritic Nanostructure Modified Electrode. From the technological point of view, it is very important to develop biosensors with high sensitivity, ease of operation, and high efficiency for dopamine detection. Recently, trends in the research and development of novel nanostructures have increasingly emphasized the application in biosensing. Although perovskite oxide nanostructures have wide and significant applications in many fields, only few reports have been focused on biomolecular detection. Herein, we report the nanostructured $LaFeO_3$ dendrite modified glassy carbon electrode for sensing dopamine (DA), ascorbic acid (AA), and uric acid (UA). Figure 10a shows cyclic voltammetric (CV) curves for the $LaFeO_3$ dendrite modified glassy carbon electrode (GCE) and the modified electrode with DA, AA, and UA recorded in 10 mM PBS (pH = 7.2) solution. To avoid the environmental effects, we measured CV curves for the solution saturated with N_2 gas.

It can be observed from Figure 10a, curve 1, that DA, AA, and UA show no redox peaks for the modified GCE. It is clear that the oxidation peak potentials of DA, AA, and UA are very close to each other for the $LaFeO_3$ dendrite modified electrode, and the electrochemical reactions are quasireversible or irreversible. For 1 μM DA (Figure 10a, curve 2), the cathodic and anodic peaks appear at −135 and 125 mV, respectively, and the peak potential separation (ΔE) is about 260 mV at the modified GCE. The oxidation peak results from the dopamine oxidation to dopaminequinone, whereas the reduction peak is caused by reducing dopaminequinone to dopamine. For 50 μM AA and 100 μM UA, the electrochemical reactions are irreversible and the signals show broader oxidation peaks with the peak potentials at 134 mV (AA, Figure 10a, curve 3) and 223 mV (UA, Figure 10a, curve 4). These indicate the sluggish electron transfer kinetics at the $LaFeO_3$ dendrites, which may be related to the nonconductive components and the electrode fouling caused by the deposition of AA, UA, and their oxidation products on the electrode surface.[41] The oxidation for DA, AA, and UA appears at 125, 134, and 223 mV, respectively. The peak potentials of DA-AA, UA-AA, and UA-DA with low oxidation peak separations of 9, 89, and 98 mV, respectively, were noticed. These separations are not sufficient enough for simultaneous determination of these species. It is observed that the concentration of DA is as low as 50 times AA and 100 times UA. The excellent selectivity of the $LaFeO_3$ dendrite modified electrode for DA can be explained as follows: The metal surface of the $LaFeO_3$ dendrite modified electrode was negatively charged. AA and UA exist as anions, and DA exists as cations. The negative surface of the metal $LaFeO_3$ dendrites attracts the cation DA and simultaneously repels AA and UA anions. Therefore, AA and UA cannot enter the $LaFeO_3$ dendrite surfaces to the same extent as DA, which is clearly evident from the redox peak at −135 mV. Therefore, the $LaFeO_3$ dendritic nanostructures exhibit strong electrocatalytic activity in response to dopamine reduction and improve the electron transfer between dopamine and the $LaFeO_3$ dendrite modified GCE.

The dopamine electrocatalytic ability of the $LaFeO_3$ dendrite modified electrode at different concentrations was obtained for further investigations. Figure 10b shows the electrocatalytic properties of $LaFeO_3$ dendrites toward the reduction of dopamine in 10 mM PBS (pH = 7.2) with a scan rate of 50 mV/s and different dopamine concentrations (1−10 μM). It can be observed that the dopamine peak current increases with the increase in dopamine concentration. A good linearity between the anodic peak current and the reaction of the electrode with dopamine was observed due to the diffusion-controlled process. From the plot of catalytic current vs the concentration of DA (Figure 10c), it was observed that the catalytic current for the oxidation of DA at modified $LaFeO_3$ dendrites was proportional to the concentration of DA in the range of 1.7×10^{-8} to 4.1×10^{-7} M and was represented by a linear equation[42] with a correlation coefficient of 0.9960. The sensitivity and the lower limit were found to 65 nM and 6.9×10^{-8} M, respectively. Figure 10d shows the linear sweep voltammograms (LSVs) obtained for DA in the concentration range of 0−100 μM at the $LaFeO_3$ dendrite modified electrode.

dx.doi.org/10.1021/cg3014305 | Cryst. Growth Des. 2013, 13, 291−302

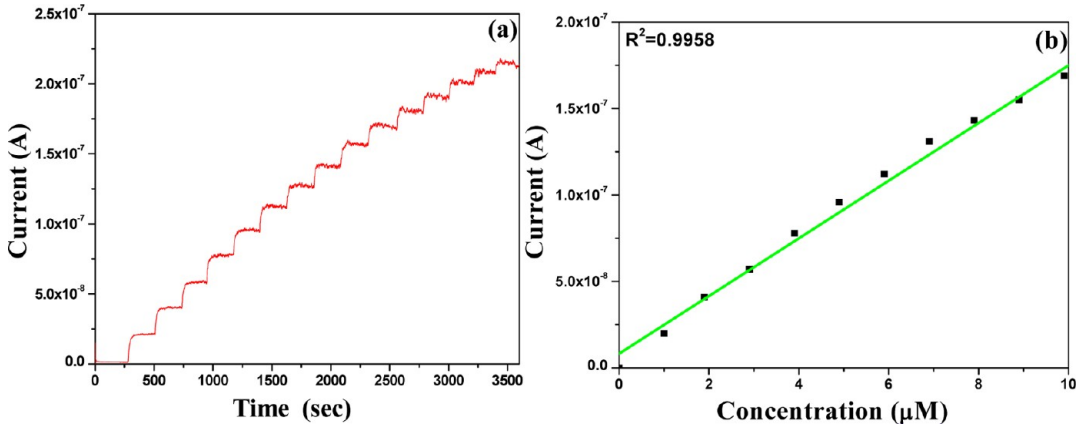

Figure 12. (a) Amperometric $i-t$ curve for the determination of DA at the $LaFeO_3$ dendrite modified electrode in 10 mM PBS 7.2. Each addition increases the concentration of 100 nM at regular intervals of 180 s. (b) Plot of the concentration of DA vs current.

The oxidation current of DA got enhanced with the increase in DA concentration (each step with the increment of 5 μM). The oxidation current has a linear relationship with the concentration of DA, with a correlation coefficient of 0.9945 (data not shown).

According to the above discussions, the redox steps involved during the cyclic voltammetric response of the $LaFeO_3$ dendrite modified electrode for dopamine sensing have been illustrated schematically in Figure 11. The electrocatalytic mechanism involves the electrochemical oxidation of Fe(III), producing the Fe(IV) complex on the surface of the electrode, followed by the electron transfer of dopamine and, consequently, regeneration of Fe(III) in the complex. The oxidation of dopamine to dopaminequinone by liberating two hydrogens can be catalyzed by the Fe(IV)/(III) redox couple in the alkaline medium, also confirmed from the oxidation and reduction peaks in Figure 10b. The following electrochemical reactions are considered as the basis for the fabrication of neurotransmitter compound sensors for electrochemical detection of dopamine during the electrooxidation mechanism

$$LaFeO_3{-}Fe(III) + OH^-_{Sol} \Leftrightarrow LaFeO_3(OH^-){-}Fe(IV) + e^- \quad (1a)$$

$$LaFeO_3(OH^-){-}Fe(IV) + \text{dopamine} \rightarrow LaFeO_3{-}Fe(III) + \text{dopaminequinone} \quad (2a)$$

The $LaFeO_3$ dendrite modified electrode exhibited high electrocatalytic activity toward dopamine oxidation, which improves the reversibility and enhances the electron-transfer kinetics. The incorporation of the Fe(IV) complex in the $LaFeO_3$ dendritic structures helped to improve the dopamine electrocatalytic activity of the modified electrode.

4.2. Amperometric Determination of DA. Furthermore, the amperometric study was performed to examine the sensitivity of the $LaFeO_3$ dendrite modified electrode toward the detection of dopamine in a homogeneously stirred 10 mM PB solution (pH 7.2), as shown in Figure 12a. The $LaFeO_3$ dendrite modified electrode shows the current response for the addition of each 100 nM DA. The current response increases and the steady-state current response were attained within 5 s for further additions of 100 nM DA in each step with a sample interval of 180 s. The dependence of response current on the concentration of DA was linear from 100 to 1500 nM with a correlation coefficient of 0.9958, as shown in Figure 12b.The amperometric $i-t$ curve for each addition of 100 nM DA showed a linear current increase without noise. It is worthy to compare the detection limit and wide linear range concentration of DA obtained in the present study with the reported different nanoparticle modified electrodes. Compared to previous reports,[43−46] the $LaFeO_3$ dendrite modified electrode showed the lowest detection limit for dopamine 62 nM with a wide range of concentration of 8.2×10^{-8} to 1.6×10^{-6} M. These results confirmed that the $LaFeO_3$ dendrite modified electrode has high selectivity and good sensitivity toward DA.

4.3. Reproducibility and Stability of Modified Electrode. The reproducibility of the $LaFeO_3$ dendrite modified electrode was evaluated at a given concentration in the linear range by cyclic voltammetric measurements. The relative standard deviations of the response of nanostructured $LaFeO_3$ dendritic biosensors at 1 μM for seven successive measurements are 3.5%, which indicates a good reproducibility. The stability of biosensors was studied by comparing the cyclic voltammetric peak currents of the $LaFeO_3$ dendritic nanostructures with the time intervals of 4 h. The decrease in the cathodic peak currents of $LaFeO_3$ biosensors immersed in PBS for 4 h was less than 3.7%, which indicates that these possess a good stability. Moreover, these biosensors can retain 98.2% of their initial response after 1 week of aging effect, which suggests good long-term stability. The excellent reproducibility and stability of $LaFeO_3$ dendrite biosensors can be attributed to the unique shape, and good biocompatibility.

5. CONCLUSION

In summary, single-crystalline $LaFeO_3$ nanostructures with a novel dendrite morphology have been successfully synthesized through a facile and efficient hydrothermal process. It is worthwhile to emphasize that the surfactant concentration and calcination temperature significantly influence the morphology of the final products. The probable reason for the formation of dendritic structures was the combined effect of diffusion-controlled aggregation and oriented attachment of the nanoparticles at favorable sites, leading to the formation of such a unique morphology. The average crystallite size was estimated to be 84 nm from XRD, and the lattice fringes were 0.27 nm along the (121) crystallographic plane of $LaFeO_3$, which was confirmed from TEM and HRTEM results. The prepared material was thermally stable, does not undergo any structural change even at higher temperature (~1000 °C), and

dx.doi.org/10.1021/cg3014305 | Cryst. Growth Des. 2013, 13, 291−302

has more adsorbed oxygen or oxygen in the hydroxyl group, confirmed from XPS. Most importantly, the obtained $LaFeO_3$ dendritic nanostructure with a high surface area exhibits high electrocatalytic ability (selectivity, sensitivity, reproducibility, and stability) for dopamine reduction when compared to that of other nanomaterials and was found to be a good candidate for application as a dopamine biosensor in analytical detection. We believe that $LaFeO_3$ nanostructures, a financially viable perovskite oxide, could be a promising material with a great potential for applications in many fields.

AUTHOR INFORMATION

Corresponding Author

*Phone: +91-422 2428423. Fax: +91-422-2422387. E-mail: ponpandian@buc.edu.in.

Notes

The authors declare no competing financial interest.

ACKNOWLEDGMENTS

S.T. gratefully acknowledges the Jawaharlal Nehru Memorial Fund for Doctoral Studies (ref: SU-A/270/2011-2012/388, dated 09-12-2010) to carry out the research.

REFERENCES

(1) Masuda, Y.; Kato, K. *Cryst. Growth Des.* **2008**, *8*, 3213−3218.
(2) Nakanishi, T.; Masuda, Y.; Koumoto, K. *Chem. Mater.* **2004**, *16*, 3484−3488.
(3) Thirumalairajan, S.; Girija, K.; Ganesh, I.; Mangalaraj, D.; Viswanathan, C.; Balamurugan, A.; Ponpandian, N. *Chem. Eng. J.* **2012**, *209*, 420−428.
(4) Masuda, Y.; Kato, K. *Cryst. Growth Des.* **2008**, *20*, 1057−1063.
(5) Cho, S. O.; Lee, E. J.; Lee, H. M.; Kim, J. G.; Kim, Y. *J. Adv. Mater.* **2006**, *18*, 60−65.
(6) Xia, Q.; Zhiying, M.; Yuxin, F.; Zhang, D.; Ma, J.; Lu, Z.; Chen, Q.; Shao, X. *Langmuir* **2012**, *28*, 5218−5226.
(7) Mohanrao, V. M.; Han, S. H.; Habib, M. P. *CrystEngComm* **2012**, *14*, 86−89.
(8) Fang, J. X.; You, H. J.; Kong, P.; Yi, Y.; Song, X. P.; Ding, B. J. *Cryst. Growth Des.* **2007**, *7*, 864−867.
(9) Duan, X.; Huang, Y.; Cui, Y.; Wang, J.; Lieber, C. M. *Nature* **2001**, *409*, 66−69.
(10) Fan, L.; Guo, R. *Cryst. Growth Des.* **2008**, *8*, 2150−2156.
(11) Rashid, H.; Mandal, T. K. *J. Phys. Chem. C* **2007**, *111*, 16750−16760.
(12) Zhang, Y.; Sun, H.; Chen, C. F. *Phys. Lett. A* **2009**, *373*, 2778.
(13) Chen, Z.; Shan, Z.; Cao, M. S.; Lu, L.; Mao, S. X. *Nanotechnology* **2004**, *15*, 365.
(14) Kuang, D.; Xu, A.; Fang, Y. P.; Liu, H. Q.; Frommen, C.; Fenske, D. *Adv. Mater.* **2003**, *15*, 1747−1750.
(15) Tangboriboon, N.; Jamieson, A. M.; Sirivtl, A.; Wongkasemjit, S. *Appl. Organomet. Chem.* **2006**, *20*, 886−894.
(16) Nathanael, A. J.; Hong, S. I.; Mangalaraj, D.; Ponpandian, N.; Chen, C. P. *Cryst. Growth Des.* **2012**, *12*, 3565−3574.
(17) Coondoo, I.; Jha, A. K. *Mater. Lett.* **2009**, *63*, 48−50.
(18) Cho, S. B.; Noh, J. S.; Lencka, M. M.; Riman, R. E. *J. Eur. Ceram. Soc.* **2003**, *23*, 2323−2335.
(19) Li, X.; Tang, C.; Ai, M.; Dong, L.; Xu, Z. *Chem. Mater.* **2010**, *22*, 4879−4889.
(20) Holmberg, K. *J. Colloid Interface Sci.* **2004**, *274*, 355−364.
(21) Wang, Y.; Gang, X.; Yang, L.; Ren, Z.; Xiao, W.; Weng, W.; Dua, P.; Ge, S.; Han, G. *J. Cryst. Growth* **2009**, *311*, 2519−2523.
(22) Gang, X.; He, W.; Zhao, Y.; Liu, Y. *CrystEngComm* **2011**, *13*, 1498−1503.
(23) Shankaran, D. R.; Limura, K.; Kato, T. *Sens. Actuators, B* **2003**, *94*, 73−80.
(24) Kong, F.; Liu, H.; Dong, J.; Qian, W. *Biosens. Bioelectron.* **2011**, *26*, 1902−1907.
(25) Mascarenhas, R. J.; Reddy, K. V.; Kumaraswamy, B. E.; Sherigara, B. S.; Lakshminarayanan, V. *Bull. Electrochem.* **2005**, *21*, 341−345.
(26) Wang, Y.; Zhu, J.; Zhang, L.; Yang, X.; Wang, X. *Mater. Lett.* **2006**, *60*, 1767−1770.
(27) Sharma, P.; Yeo, J.; Kim, D. M.; Cho, C. H. *J. Mater. Chem.* **2012**, *22*, 2838−2843.
(28) Farhadi, S.; Momeni, Z.; Taherimehr., M. *J. Alloys Compd.* **2009**, *471*, L5−L8.
(29) Popa, M.; Frantti, J.; Kakihana, M. *Solid State Ionics* **2002**, *154*−*155*, 437−445.
(30) Wei, Z. X.; Xu, Y. H.; Liu, H. Y.; Hu, C. H. *J. Hazard. Mater.* **2009**, *165*, 1056−1061.
(31) Su, H.; Jing, L.; Shi, K.; Yao, C.; Fu, H. *J. Nanopart. Res.* **2010**, *12*, 967−975.
(32) Rida, K.; Benabbas, A.; Bouremmad, F.; Pena, M. A.; Sastre, E.; Martinez, A. *Appl. Catal., A* **2007**, *327*, 173−179.
(33) Mickevicius, S.; Grebinskij, S.; Bondarenka, V.; Vengalis, B.; Sliuziene, K. *J. Alloys Compd.* **2006**, *423*, 107−111.
(34) Qi, X.; Zhou, J.; Yue, Z.; Gui, Z.; Longtu, L. *Mater. Chem. Phys.* **2002**, *78*, 25−29.
(35) Cao, M.; Liu, T.; Gao, S.; Sun, G.; Wu, X.; Hu, C.; Wang, Z. *Angew. Chem., Int. Ed.* **2005**, *44*, 4197−4201.
(36) Wang, Y.; Xu, G.; Yang, L.; Ren, Z. *J. Cryst. Growth* **2009**, *311*, 2519−2523.
(37) Yaping, H.; Zheng, J.; Sheng, Q. *Analyst* **2012**, *137*, 1031−1038.
(38) Yang, H. G.; Zeng, H. C. *J. Phys. Chem. B* **2004**, *108*, 3492−3495.
(39) Witten, T. A.; Sander, L. M. *Phys. Rev. Lett.* **1981**, *47*, 14001403.
(40) Fleury, V. *Nature* **1997**, *390*, 145.
(41) Safavi, A.; Maleki, N.; Moradlou, O.; Tajabadi, F. *Anal. Biochem.* **2006**, *359*, 224−229.
(42) Babu, R. S. *Colloids Surf., B* **2011**, *88*, 755−763.
(43) Bergamini, M. F.; Santos, A. L.; Stradiotto, N. R.; Zanoni, M. V. B. *J. Pharm. Biomed. Anal.* **2005**, *39*, 54−59.
(44) Teixeira, M. F. S.; Marcolino-Junior, L. H.; Fatibello-Filho, O.; Dockal, E. R.; Bergamini, M. F. *Sens. Actuators, B* **2007**, *122*, 549−555.
(45) Wang, G.; Sun, J.; Zhang, W.; Jiao, S.; Fang, B. *Microchim. Acta* **2009**, *164*, 357−362.
(46) Mathiyarasu, J.; Nyholm, L. *Electroanalysis* **2010**, *22*, 449−454.